An Innovative CCD-Based High-Resolution CT System for Analysis of Trabecular Bone Tissue

F. Baruffaldi, M. Bettuzzi, D. Bianconi, R. Brancaccio, S. Cornacchia, N. Lanconelli, L. Mancini, M. P. Morigi, A. Pasini, E. Perilli, D. Romani, A. Rossi, and F. Casali

Abstract—Synchrotron-based digital radiography and microtomography devices are powerful, nondestructive, high-resolution research tools. In this paper, we present a linear system with a pixel size of 22.5 μm and a field-of-view (FOV) 13 cm long and about 1 mm high. The system is composed of a linear converter GOS screen coupled to an intensified electron-bombarded CCD (EBCCD) camera, by means of a rectangular-to-linear fiber optic adapter. This optical guide is composed of seven bundles, each one transporting light in a coherent way to preserve spatial information. In this way, a high spatial resolution over an extended FOV is obtained. The detector works as an X-ray scanner by means of a high-precision translation mechanical device with 18 cm travel range. The total FOV obtained this way is 13 cm long and 18 cm high. The aim of this paper is to demonstrate the feasibility of this system to investigate a large area of a bone and to calculate the appropriate histomorphometric parameters. Here we present an investigation gained at ELETTRA synchrotron facility at Trieste, Italy. A monochromatic 34-keV beam has been used for imaging a human proximal femur, about 9 cm in width, with our system. The reconstructed images (13 cm $\times$ 13 cm) were cross sections containing femoral head, femoral neck, and greater trochanter. The local variations in trabecular and cortical structure of the examined bone were clearly visible at a level not obtainable with medical CT scanners. The used spatial resolution allowed the visualization of thin trabeculae, which typically lie in a range of 100 μm or lower. The quality of the reconstructed cross-section images confirmed that the system presented is a novel tool for high resolution three-dimensional (3-D) imaging of bone structure, with a pixel size over a volume of interest not achievable with conventional microCT scanners.

Index Terms—Biomedical, X-ray detectors, X-ray tomography.

I. INTRODUCTION

MICROCOMPUTED TOMOGRAPHY (microCT) and digital radiography are nondestructive techniques which provide high-resolution images of the internal structures of the investigated objects. In addition, microCT images can be elaborated for the realization of high-resolution three-dimensional (3-D) digital reconstructions and models. Such 3-D reconstructions can be used to visualize inner structures and details, to investigate fine morphological variation, to perform advanced morphometric analyses.

Osteoporosis is a major health problem and the possibility of predicting the risk of fracture is vital for patients. It is a destructive process occurring in bones, characterized by a loss of bone mass and degeneration of the bone microstructure. Bone strength depends on bone quality, which is commonly assessed by measuring the bone mineral density (BMD) using dual energy X-ray absorptiometry (DEXA). The BMD gives information about the amount of mineralized tissue that is present, which is due to the cortical shell and to the trabecular bone. Unfortunately, BMD gives no information about the spatial arrangement of the bone microstructure, e.g., the spatial distribution of the trabeculae and of the cortical microporosities.

The fracture risk is strongly correlated with the loss of bone mass, but there are patients with low bone mass which do not suffer from osteoporotic fractures [1]–[3]. Therefore many investigators searched for factors others than low bone mass, as changes in geometric structure, accumulated microdamage and differences in tissue properties to explain the occurrence of fracture in some osteoporotics and not in others. [4]–[11]

A number of studies showed the mechanical properties of bone to be correlated to the trabecular microstructure [12]–[14]. The architectural structure of bone can be investigated with high accuracy through histological sectioning in human biopsies. However, this method is invasive and necessitates a mechanical cutting of the object to be investigated at the microscope. A substantial number of recent studies have focused on imaging the microstructure of the bone in critical areas of the skeleton. To this end, microCT can be used as a nondestructive technique for analyzing the microstructure of trabecular bone, thanks to its high spatial resolution [15]–[19].

Synchrotron radiation X-ray sources offer high photon intensity, good collimation and a broad continuous energy range from which almost any desired spectral region can be selected with a very high resolution in energy. Synchrotron radiation pushes high-resolution examinations to the micrometer range. In addition, the use of a monochromatic source improves tomography examinations, by eliminating beam-hardening artifacts. For these reasons, tremendous efforts are made all over the world to develop synchrotron-based microtomography devices. However, these systems usually include a small field of view, in the order of some centimeters, suitable for studies over
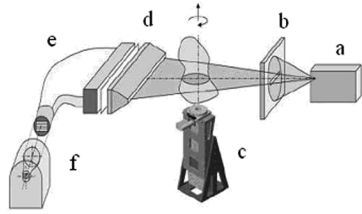
Fig. 1. Sketch of the experimental setup, from right to left. (a) X-ray source. (b) Collimator. (c) Object manipulator. (d) GOS converter screen. (e) Linear-to-rectangular fiber optic adapter. (f) EBCCD camera.
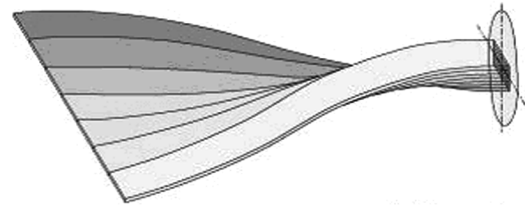

Fig. 2. Linear-to-rectangular fiber optic adapter, composed of seven bundles: the linear input face on the left is converted into a rectangular exit on the right.

bone samples of small animals, as rats or mice [18]. Especially for large bones, as human bones, the samples are required to be sectioned or cored [20]–[23], a delicate operation which can remove key structures from the study.

The main purpose of this paper is to investigate the performance of a CCD-based system with a pixel size of 22.5 μm and a field of view (FOV) 13-cm long and about 1 mm high. This is obtained by using a distinctive fiber-optic ribbon, which converts a linear geometry to a rectangular one. The system has been patented by the University of Bologna and already been used and tested for nonmedical applications [24]–[26]. In this paper. a CT scan of a human proximal femur is presented. The high spatial resolution of our system together with its large FOV allow the analysis of the microstructure of an entire bone, without the need of coring of small samples, in order to investigate changes in the trabecular structure caused by osteoporosis. We aim to demonstrate that with our system we are able to analyze at high resolution and in a nondestructive way a large area of the bone, which usually is not achievable with common microCT or medical CT scanners, and calculate appropriate histomorphometric parameters.

II. MATERIALS AND METHODS

A. Description of the System

The essential components for a microCT system are a microfocus (or a synchrotron) X-ray source, a precise object manipulator, and a high resolution X-ray detector. Our system is composed of a sample-handler consisting of a rotation and translation stage. The object can be translated in z direction and rotated with high positional accuracy. A two dimensional radiography can therefore be obtained, by translating the object in front of the linear detector. The maximum scanning length is limited to 18 cm by the mechanical travel range. The object manipulation, data acquisition, image processing and reconstruction steps are controlled by a common PC. In Fig. 1(a) sketch of the entire system is depicted.

The detector consists of a linear converter screen (gadolinium oxysulfide, GOS), a linear-to-rectangular fiber optic adapter, and an intensified electron-bombarded CCD (EBCCD) camera. The linear GOS screen has a front area equal to 129 mm × 1.45 mm and converts the X-rays into visible light, which is transported to the EBCCD camera by means of the linear-to-rectangular fiber optic adapter. The fiber optic adapter (Fig. 2) is composed of seven bundles, each one made of glass microfibers transporting light in a coherent way to preserve spatial information. In this way, a high spatial resolution over an extended
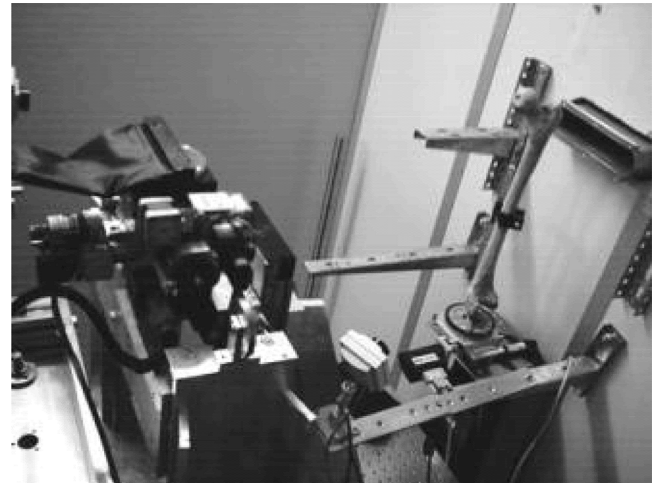

Fig. 3. Experimental setup at ELETTRA: the linear detector (on the left), the human femur sample (on the right), and the X-ray synchrotron exit window (on the extreme right).

FOV is obtained. The EBCCD camera acts as an image intensifier provided with an intrinsic digitizer.

The main feature of the presented system is its high spatial resolution, thanks to the pixel size of about 22.5 μm, even for large objects (up to 13 cm). The high sensitivity of the EBCCD camera allows the use of a low radiation intensity and a significant response also with a short exposure time. In addition, the linear geometry is appropriate for beam collimation and a further reduction in scattered radiation, leading to a better image contrast. More details about the system are given in the Appendix. A complete characterization of this CT system was described elsewhere in our previous works [25], [26].

B. CT System at Elettra

Here we present a tomographic investigation gained at ELETTRA synchrotron facility at Trieste, Italy, at SYnchrotron Radiation for MEdical Physics (SYRMEP) beamline. The SYRMEP beamline has been designed for research in medical diagnostic radiology. In this case, a monochromatic 34-keV beam was used for imaging a proximal femur with our system. For this CT system, the motion control includes rotational and vertical translation stages (Fig. 3).

The analyzed bone is a human dried femur and has a maximum width of about 9 cm. Therefore, it is possible to get a digital radiography of the object with a scanning of the linear detector (maximum FOV equal to 13 cm × 18 cm). In order to reduce the noise contribution, each single slice was obtained by averaging 16 consecutive frames.

TABLE I
ACQUISITION PARAMETERS USED FOR THE PRESENT STUDY

Beam energy	34 keV
Source-to-Object distance	24 m
Object-to-Detector distance	55 cm
Exposure time per single frame	25 ms
# of averaged frames	16

Fig. 4. Medical radiographic image of the examined femur. The two lines show the different heights at which the two CT scans were performed. The histomorphometric analysis were done on ROIs within the lower scan line.

Table I summarizes the main parameters used for the acquisition of the femur at the ELETTRA synchrotron beamline. The same parameters were used both for radiographic and tomographic inspections. The CT slices were obtained by using a standard parallel beam reconstruction algorithm. The image reconstruction time was 1 min per slice on a Pentium IV 2.6-GHz based PC.

C. The Sample Examination

The scanned bone was a human femur taken from the didactic archive of the Rizzoli Institute, Bologna, Italy. The femur, obtained from a human cadaver, was fixed in ethanol 70% for one month. On the greater trochanter the bone presented a small damage in the cortex. A clinician evaluated the femur having Singh Index 5 (Singh Index 0 stays for severe osteoporosis, 6 for normal [27]) from a medical RX image (Fig. 4).

The proximal part of the femur was scanned two times, about 9 cm in width and 1 mm in height each. Each scan produced a stack of 50 tomographic slices (total height equal to about 1 mm), in order to assess the feasibility of using this system for analyzing the trabecular structure of the femur. The first scan, named upper scan, contained femoral head and greater
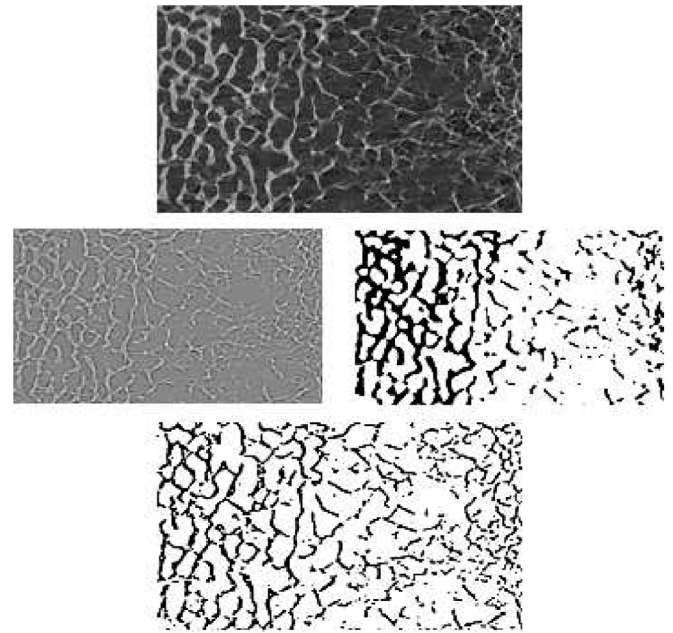

Fig. 5. The enhanced method used for the segmentation. Top row: raw reconstructed image. Middle row: left—enhanced image, right—global threshold of the raw image. Bottom row: binary image after logical AND operation between images shown on the middle row and suppression of the isolated points.

trochanter; the second, named lower scan, contained femoral neck and greater trochanter.

D. Extraction of the Bone Parameters

In order to perform calculations of the bone parameters an edge enhancement segmentation was used. This technique is based on a combination of edge enhancement and histogram segmentation. It consists in clustering pixels with the respect to both a homogeneity criterion and an adjacent criterion. Basically, the raw image is first segmented with a global threshold method. On the other hand, the same raw image is filtered with a high-pass filter, in order to get a more precise description of the trabecular regions. The high-pass filtered image is then segmented with the same global segmentation used for the raw image. These two segmented images are then combined with a logical AND operation and finally isolated pixels are removed. Fig. 5 illustrates images obtained at the various steps of the edge-enhanced method.

In the reconstructed cross sections of the lower scan a rectangular region of interest (ROI), named Big ROI (22 mm × 13 mm) was placed inside the femoral neck for histomorphometric analysis. Two smaller ROIs, named Left ROI and Right ROI were then considered within the selected Big ROI. The sizes of these ROIs were 8.5 mm × 13 mm and 10 mm × 13 mm, respectively, for Left ROI and Right ROI.

The parameters for the trabecular characterization are bone volume fraction (BV/TV), trabecular thickness (Tb.Th), trabecular separation (Tb.Sp), and trabecular number (Tb.N), calculated using the plate model, following the recommendations of the American Society of Bone and Mineral Research [28]. The BV/TV is the number of pixels recognized as bone divided by the number of pixels constituting the ROI. The parameter Tb.Th is the mean thickness of the trabeculae expressed in micron, the
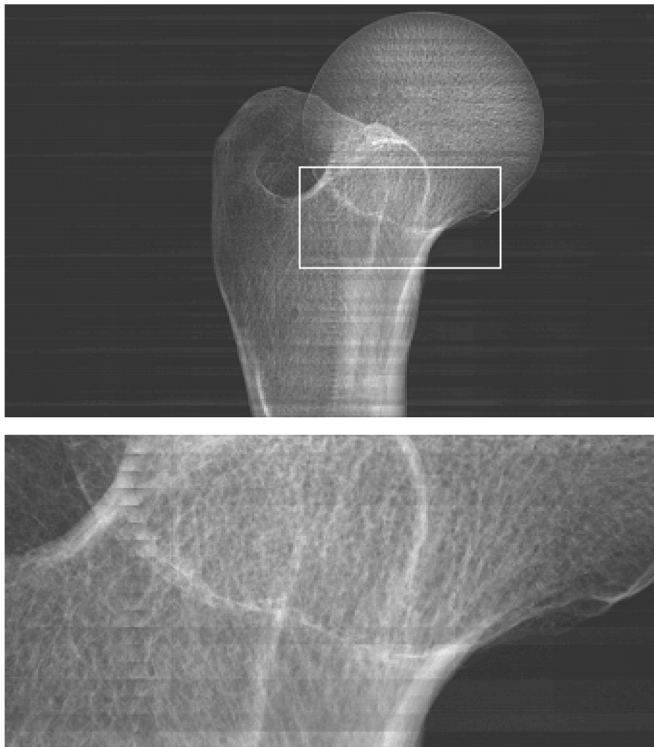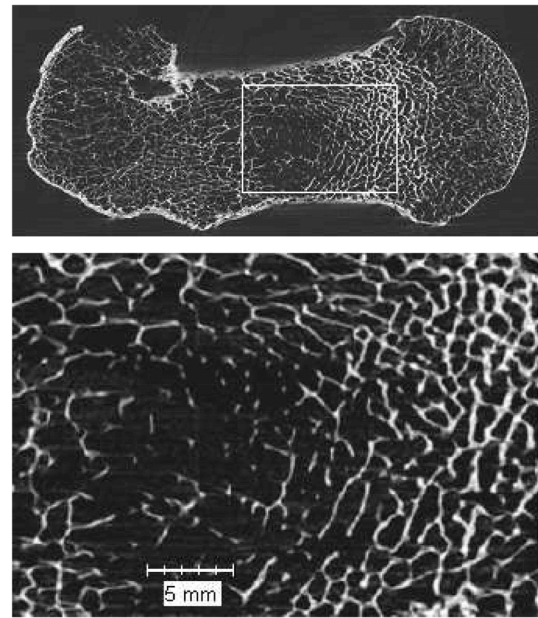
Fig. 7. Reconstructed tomographic slice of the human femur: the trabecular structure is clearly visible over the entire FOV. Top: entire FOV. Bottom: enlargement of the box shown above.

Fig. 6. Digital radiography of the human femur obtained with the presented system: in this case the FOV is about 13 cm (width) × 8 cm (height). Top: entire FOV. Bottom: enlargement of the box shown above.

parameter Tb.Sp is the mean distance between the edges of the trabeculae expressed in micron, while Tb.N is the mean number of trabeculae per unit length expressed in mm^{-1} [28].

The conventionally available microCT systems can reach high spatial resolutions, but on the other hand they can only investigate areas limited to few centimeters side [15]–[17], [29]–[31]. Conversely, thanks to the large cross-sectional area (13 cm × 13 cm) that we are able to inspect with the presented system, it is possible to perform calculations of the histomorphometric parameters in big and in small areas, by choosing arbitrary ROIs that are larger than the FOV of usually available systems.

III. RESULTS

Fig. 6 shows a digital radiography of the upper part of the femur. This radiography was obtained from a stack of acquired frontal images, keeping the femur in a fixed rotational position and shifting it in the longitudinal direction. The total scanning time required for the whole projection was about 600 s, comprising exposure time, acquisition time, and time for mechanical shifting. The trabecular structure is clearly identified over the entire FOV. That allowed the investigation of 3-D bone architecture and the study of histomorphometric parameters. The enlargement of a region inside the radiography confirms the great capability of the system of showing very tiny structures within the femur.

In Fig. 7, an example of a reconstructed tomographic slice obtained in the CT scan (lower scan line) is shown. It can be clearly seen that the system is capable to image thin trabecular structures over the whole cross-sectional area. This is due both

to the good characteristics of the system and to the use of a synchrotron beam. The pixel size used here is comparable to the one currently achievable with commercial microCT systems, but those have FOV limited up to a couple of centimeters. The use of the fiber-optic converter allowed us to extend the spatial resolution to a width greater than 10 cm. In literature it is reported that although only the highest resolution will predict the correct values, a pixel size up to 100 μm is sufficient for the quantitative description (in terms of BV/TV, Tb.N, Tb.Th, Tb.Sp) of the trabecular bone structure [32]. Thus, the pixel size of 22.5 μm used in the present study is more than adequate.

The two lines shown in Fig. 4 indicate the cross sections presented in Fig. 8 (the upper and the lower scan shown on the top and on the bottom of the figure, respectively). The reconstructed cross sections show local variations in the trabecular and cortical structure of the examined bone at a pixel size not obtainable with medical CT scanners (the typical pixel size for those systems lies in the range of 500 μm to 1000 μm, even if in literature special cases of 150 μm and 200 μm are reported [33], [34]). Also the damage in the cortical bone is clearly observable (Fig. 8 - upper scan).

The histomorphometric calculations were done over 50 slices acquired for the lower scan. Table II summarizes the parameters obtained in the Big ROI placed in the femoral neck.

Two smaller ROIs (Left ROI, Right ROI) were selected within the Big ROI, as highlighted in Fig. 8. Visually, these ROIs are characterized by a different structure: the left ROI shows a thicker and larger amount of trabecular structure than the Right ROI. Fig. 9 shows the segmented images of the two ROIs and Table III summarizes the parameters computed on them. The calculated parameters show a higher bone volume fraction, larger trabecular thickness and trabecular number in the left ROI, whilst the trabecular separation is larger for the right ROI. Once again, we would like to stress that with the
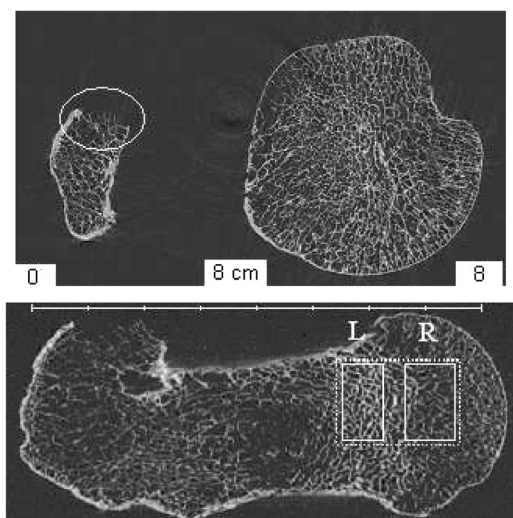
Fig. 8. MicroCT reconstruction of the two scans highlighted on Fig. 4. Top: upper scan. The damage in the cortical bone at the trochanteric site is clearly visible (outlined by an ellipse). Bottom: lower scan. Here, the three ROIs used for the histomorphometric calculation are shown (Big ROI with dashed line, Left ROI - L, and Right ROI - R, both with solid lines).

TABLE II
AVERAGE HISTOMORPHOMETRIC PARAMETERS OF
THE BIG ROI CALCULATED OVER 50 SLICES

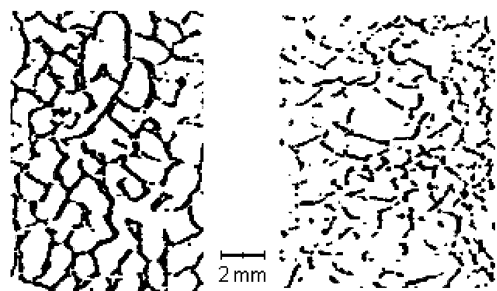|	BV/TV [%]	Tb.Th [μm]	Tb.N [mm^{-1}]	Tb.Sp [μm]
Big ROI	17.5±0.2	122±2	1.44±0.02	576±8

Fig. 9. Left and Right ROI where the histomorphometric parameters shown in Table III were calculated.

TABLE III
AVERAGE HISTOMORPHOMETRIC PARAMETERS OF LEFT AND RIGHT ROI
CALCULATED OVER 50 SLICES

	BV/TV [%]	Tb.Th [μm]	Tb.N [mm^{-1}]	Tb.Sp [μm]
Left ROI	21.4±0.3	167±2	1.28±0.03	610±20
Right ROI	13.8±0.2	120±1	1.17±0.02	740±10

reconstruction of the entire FOV achieved with the present system it is possible to calculate the parameters on any arbitrary ROI in the femur, keeping it intact.

The reconstructed data from the 50 slices obtained in the lower scan were finally combined into a unique volume Fig. 10
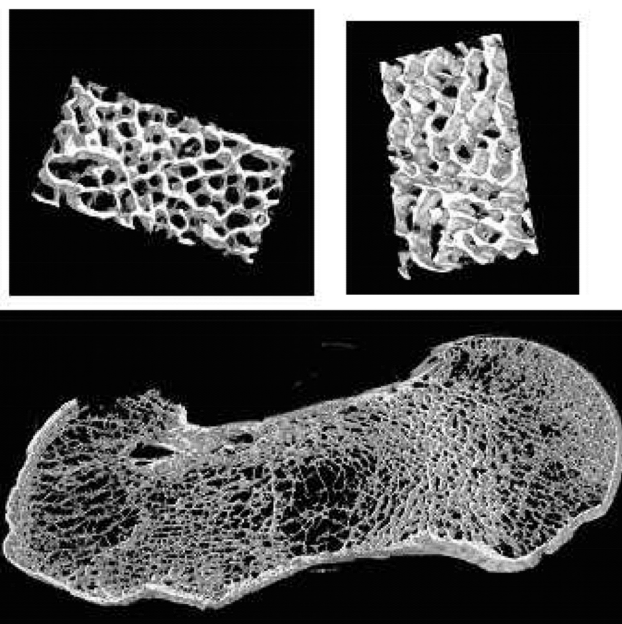

Fig. 10. Three-dimensional images obtained from a stack of 50 microCT slices of the examined human femur. Top row: two particulars of an ROI. Bottom row: reconstruction of the entire cross-sectional area.

shows examples of the rendering obtained over the volume of a single ROI and of the entire reconstructed cross-sectional area.

IV. CONCLUSION

A high-resolution CT system with 22.5 μm pixel size and FOV of 13 cm × 18 cm was set up for a synchrotron source. The possibility of analyzing a sample of large size permits the reconstruction of CT slices of big parts of bones or even complete bones (i.e., proximal femur, wrist), leaving them intact and without special sample preparation (i.e., specimen cutting, extraction). We demonstrated the feasibility of using such images to extract information about the trabecular structure by scanning the proximal part of a human femur, containing greater trochanter, femoral neck, and femoral head.

This system is an improvement with respect to standard microCT systems, since it gives the possibility to have data on a complete bone and not just in a limited ROI. The spatial limits (specimen size) were overcome in the present system because of the use of a special fiber optic adapter. The linear pixel size used (22.5 μm) is optimal for the imaging of trabecular bone structure.

The quality of the reconstructed cross-section images confirms that this investigation technique permits high-resolution 3-D imaging of large volumes (up to 18 cm × 13 cm × 13 cm) at a pixel size not achievable with conventional microCT scanners.

In the near future, we are planning to test the system with regular X-ray microfocus tubes, in order to assess the practicability of performing *in vivo* imaging of human patients.

APPENDIX

Here we provide further details about our CT system and the femur investigation accomplished at ELETTRA beamline.

With our manipulator we can perform not only a rotational scanning, but also other motions such as helical scanning. In fact, the scanner has two acquisition modes:

1) tiled-mode: CT data for a small vertical segment is acquired with rotation-only scanning, and then the sample is translated to a new vertical position;
2) spiral-CT mode: a two-dimensional image is acquired with simultaneous vertical and rotational movement.

The fiber optic adapter is made of glass microfibers, each one with a diameter of about 20 μm. The microscopic size of the fibers provides a great flexibility to the adapter. The bundles are aligned on the input face, by thus allowing a linear scanning geometry. On the other hand, the fiber-optic bundles are stacked at the exit, in order to fit the shape of the photocathode of the EBCCD camera.

We give now some details about the EBCCD camera. The CCD chip of the EBCCD camera is a special back thinned CCD (about 10 micrometers thick), with 1024×512 pixels. The EBCCD camera has a vacuum tube with an intense electric field (6 kV in our case), to accelerate electrons emitted by the photocathode. Unlike traditional Image Intensifiers, in the EBCCD only one radiation conversion takes place, since accelerated electrons are here directly detected by the CCD. As a result, high efficiency and gain are obtained. The signal is digitized through a 12-bit ADC mounted onboard on the EBCCD camera. The camera provides one digital output provided to the PC through an RS-422 digital interface and one control signal. The digital electronics of the EBCCD camera has been developed at Geosphaera Research Center in Moscow and is based on a microprocessor produced by Altera Corporation. An additional control card named ST-card is provided as a synchronization card: it generates a trigger signal, an exposition signal and a gate signal for the EBCCD. The synchronization with ST-card may reduce noise and electrical interference due to 50 Hz frequency fluctuations. A Matrox Pulsar frame grabber mounted on the PC is then used as digital data transfer and communication device between the camera and the computer. MIL Lite Matrox libraries were used to develop our in-house software for controlling the camera and the other devices of the system.

The SYRMEP beamline at ELETTRA is characterized by an optics system based on a double-crystal Si monochromator that works in an energy range between 8 and 35 keV. The beamline provides at a distance of about 20 m from the source, a monochromatic, laminar-section X-ray beam with a maximum area of 120 mm $\times$ 4 mm. For the present femur investigation, the exposure time for each frame was fixed to 25 ms. The acquisition was done with 2800 projections over 180 degrees. The total scan time over 180 degrees for a 1–mm-thick slice was about 3.5 h (comprising exposure time, acquisition time, and time for rotation).

REFERENCES

[1] L. J. Melton, S. H. Kan, M. A. Frye, H. W. Wahner, W. M. O'Fallon, and B. L. Riggs, "Epidemiology of vertebral fractures in women," *Am. J. Epidemiol*, vol. 129, no. 5, pp. 1000–1011, 1989, 3rd.

[2] E. Legrand, D. Chappard, C. Pascaretti, M. Duquenne, S. Krebs, V. Rohmer, M. F. Basle, and M. Audran, "Trabecular bone microarchitecture, bone mineral density, and vertebral fractures in male osteoporosis," *J. Bone Miner. Res.*, vol. 15, no. 1, pp. 13–9, 2000.

[3] B. R. McCreadie and S. A. Goldstein, "Biomechanics of fracture: Is bone mineral density sufficient to assess risk?," *J. Bone Miner. Res.*, vol. 15, no. 12, pp. 2305–2308, 2000.

[4] S. L. Hui, C. W. Slemenda, and C. C. Johnston Jr, "Age and bone mass as predictors of fracture in a prospective study," *J. Clin. Invest.*, vol. 81, no. 6, pp. 1804–1809, 1988.

[5] D. B. Burr, M. R. Forwood, D. P. Fyhrie, R. B. Martin, M. B. Schaffler, and C. H. Turner, "Bone microdamage and skeletal fragility in osteoporotic and stress fractures," *J. Bone Miner. Res.*, vol. 12, no. 1, pp. 6–15, 1997.

[6] S. Mori, R. Harruff, W. Ambrosius, and D. B. Burr, "Trabecular bone volume and microdamage accumulation in the femoral heads of women with and without femoral neck fractures," *Bone*, vol. 21, no. 6, pp. 521–526, 1997.

[7] L. D. Hordon, M. Raisi, J. E. Aaron, S. K. Paxton, M. Beneton, and J. A. Kanis, "Trabecular architecture in women and men of similar bone mass with and without vertebral fracture: I. Two-dimensional histology," *Bone*, vol. 27, no. 2, pp. 271–276, 2000.

[8] J. E. Aaron, P. A. Shore, R. C. Shore, M. Beneton, and J. A. Kanis, "Trabecular architecture in women and men of similar bone mass with and without vertebral fracture: II. Three-dimensional histology," *Bone*, vol. 27, no. 2, pp. 277–282, 2000.

[9] A. J. Bailey, T. J. Sims, E. N. Ebbesen, J. P. Mansell, J. S. Thomsen, and L. Mosekilde, "Age-related changes in the biochemical properties of human cancellous bone collagen: Relationship to bone strength," *Calcif Tissue Int.*, vol. 65, no. 3, pp. 203–210, 1999.

[10] T. E. Ciarelli, D. P. Fyhrie, M. B. Schaffler, and S. A. Goldstein, "Variations in three-dimensional cancellous bone architecture of the proximal femur in female hip fractures and in controls," *J. Bone Miner. Res.*, vol. 15, no. 1, pp. 32–40, 2000.

[11] J. Homminga, B. R. McCreadie, T. E. Ciarelli, H. Weinans, S. A. Goldstein, and R. Huiskes, "Cancellous bone mechanical properties from normals and patients with hip fractures differ on the structure level, not on the bone hard tissue level," *Bone*, vol. 30, no. 5, pp. 759–764, 2002.

[12] M. J. Ciarelli, S. A. Goldstein, J. L. Kuhn, D. D. Cody, and M. B. Brown, "Evaluation of orthogonal mechanical properties and density of human trabecular bone from the major metaphyseal regions with materials testing and computed tomography," *J. Orthop. Res.*, vol. 9, no. 5, pp. 674–682, 1991.

[13] R. W. Goulet, S. A. Goldstein, M. J. Ciarelli, J. L. Kuhn, M. B. Brown, and L. A. Feldkamp, "The relationship between the structural and orthogonal compressive properties of trabecular bone," *J. Biomech.*, vol. 27, no. 4, pp. 375–389, 1994.

[14] D. Ulrich, T. Hildebrand, B. Van Rietbergen, R. Muller, and P. Ruegsegger, "The quality of trabecular bone evaluated with micro-computed tomography, FEA and mechanical testing," *Bone Res. Biomechan.*, pp. 97–111, 1997.

[15] L. A. Feldkamp, S. A. Goldstein, A. M. Parfitt, G. Jesion, and M. Kleerekoper, "The direct examination of three-dimensional bone architecture in vitro by computed tomography," *J. Bone Miner. Res.*, vol. 4, no. 1, pp. 3–11, 1989.

[16] J. L. Kuhn, S. A. Goldstein, L. A. Feldkamp, R. W. Goulet, and G. Jesion, "Evaluation of a microcomputed tomography system to study trabecular bone structure," *J. Orthop. Res.*, vol. 8, no. 6, pp. 833–42, 1990.

[17] R. Muller, H. Van Campenhout, B. Van Damme, G. Van Der Perre, Dequeker, T. Hildebrand, and P. Ruegsegger, "Morphometric analysis of human bone biopsies: a quantitative structural comparison of histological sections and micro-computed tomography," *Bone*, vol. 23, no. 1, pp. 59–66, 1998.

[18] M. Tzaphlidou, R. Speller, G. Royle, J. Griffiths, A. Olivo, S. Pani, and R. Longo, "High resolution Ca/P maps of bone architecture in 3D synchrotron radiation microtomographic images," *Appl. Radiat. Isot.*, vol. 62, no. 4, pp. 569–575, 2005.

[19] M. Sato, M. Westmore, Y. L. Ma, A. Schmidt, Q. Q. Zeng, E. V. Glass, J. Vahle, R. Brommage, C. P. Jerome, and C. H. Turner, "Teriparatide [PTH(1-34)] strengthens the proximal femur of ovariectomized non-human primates despite increasing porosity," *J. Bone Miner. Res.*, vol. 19, no. 4, pp. 623–629, 2004.

[20] F. Peyrin, M. Salome, P. Cloetens, A. M. Laval-Jeantet, E. Ritman, and P. Ruegsegger, "Micro-CT examinations of trabecular bone samples at different resolutions: 14, 7 and 2 micron level," *Technol. Health Care*, vol. 6, no. 5–6, pp. 391–401, 1998.

[21] J. H. Kinney and A. J. Ladd, "The relationship between three-dimensional connectivity and the elastic properties of trabecular bone," *J. Bone Miner. Res.*, vol. 13, no. 5, pp. 839–845, 1998.

[22] E. Bossy, M. Talmant, F. Peyrin, L. Akrout, P. Cloetens, and P. Laugier, "An in vitro study of the ultrasonic axial transmission technique at the radius: 1-MHz velocity measurements are sensitive to both mineralization and intracortical porosity," *J. Bone Miner. Res.*, vol. 19, no. 9, pp. 1548–1556, 2004.

[23] S. Nuzzo, M. H. Lafage-Proust, E. Martin-Badosa, G. Boivin, T. Thomas, C. Alexandre, and F. Peyrin, "Synchrotron radiation microtomography allows the analysis of three-dimensional microarchitecture and degree of mineralization of human iliac crest biopsy specimens: effects of etidronate treatment," *J. Bone Miner. Res.*, vol. 17, no. 8, pp. 1372–1382, 2002.

[24] A. Pasini, M. Bettuzzi, R. Brancaccio, S. Cornacchia, M. Giordano, M. P. Morigi, D. Romani, and F. Casali, "A new system for digital radiography and computed tomography with an intensified linear array detector," in *Proc. Int. Symp. CT and IP for Indust. Radiol.*, Berlin, 2003.

[25] M. Bettuzzi, S. Cornacchia, M. Rossi, E. Paltrinieri, M. P. Morigi, R. Brancaccio, D. Romani, and F. Casali, "A new linear array detector for high resolution and low dose digital radiography," *Nucl. Instrum. Methods Phys. Res. B*, vol. 213, pp. 227–230, 2004.

[26] M. Rossi, F. Casali, M. Bettuzzi, M. P. Morigi, D. Romani, S. V. Golovkin, and V. N. Govorun, "An experimental micro-CT system for X-ray NDT," in *Proc. SPIE 4503*, 2001, pp. 338–348.

[27] M. Singh, A. R. Nagrath, and P. S. Maini, "Changes in trabecular pattern of the upper end of the femur as an index of osteoporosis," *J. Bone Joint Surg.*, vol. 52A, pp. 457–467, 1970.

[28] A. M. Parfitt, M. K. Drezner, F. H. Glorieux, J. A. Kanis, H. Malluche, P. J. Meunier, S. M. Ott, and R. R. Recker, "Bone histomorphometry: Standardization of nomenclature, symbols and units. Report of the ASBMR histomorphometry nomenclature comittee," *J. Bone Miner. Res.*, vol. 2, no. 6, pp. 595–610, 1987.

[29] A. Y. Sasov, "Microtomography. part 1: Methods and equipment," *J. Microsc.*, vol. 147, no. 2, pp. 169–178, 1987.

[30] P. Ruegsegger, B. Koller, and R. Muller, "A microtomographic system for the nondestructive evaluation of bone architecture," *Calcif Tissue Int.*, vol. 58, no. 1, pp. 24–29, 1996.

[31] A. Sasov and D. Van Dyck, "Desktop X-ray microscopy and microtomography," *J. Microsc.*, vol. 191, no. 2, pp. 151–158, 1998.

[32] R. Muller, B. Koller, T. Hildebrand, A. Laib, S. Gianolini, and P. Ruegsegger, "Resolution dependency of microstructural properties of cancellous bone based on three-dimensional mu-tomography," *Technol. Health Care*, vol. 4, no. 1, pp. 113–119, 1996.

[33] E. Cendre, D. Mitton, J. P. Roux, M. E. Arlot, F. Duboeuf, B. Burt-Pichat, C. Rumelhart, G. Peix, and P. J. Meunier, "High-resolution computed tomography for architectural characterization of human lumbar cancellous bone: Relationships with histomorphometry and biomechanics," *Osteoporos. Int.*, vol. 10, no. 5, pp. 353–360, 1999.

[34] B. Cortet, D. Chappard, N. Boutry, P. Dubois, A. Cotten, and X. Marchandise, "Relationship between computed tomographic image analysis and histomorphometry for microarchitectural characterization of human calcaneus," *Calcif Tissue Int.*, vol. 75, no. 1, pp. 23–31, 2004.